

Primljen / Received: 22.3.2021.

Ispravljen / Corrected: 22.8.2023.

Prihvaćen / Accepted: 15.12.2023.

Dostupno online / Available online: 10.6.2024.

# Mechanical behavior of rock mass under simulated materials shear testing

## Authors:

Prof. **Xing-Chao Lin**, PhD. CEState Key Laboratory of Simulation and Regulation of Water Cycle in River Basin, China  
[linxc@iwhr.com](mailto:linxc@iwhr.com)

Corresponding author



Gui-Na Zhu, MSc. CE

Beijing Glory PKPM Technology Co., China  
[zhuguina@cabrtech.com](mailto:zhuguina@cabrtech.com)

Xing-Song Sun, PhD. CE

State Key Laboratory of Simulation and Regulation of Water Cycle in River Basin, China  
[sunxs@iwhr.com](mailto:sunxs@iwhr.com)

Research Paper

**Xing-Chao Lin, Gui-Na Zhu, Xing-Song Sun**

## Mechanical behavior of rock mass under simulated materials shear testing

In this paper, the influence of joint distribution on the deformation and strength characteristics of rock mass is studied through direct shear tests of five typical distribution types of simulated materials including two joints. The spatial distribution pattern of joints determines the deformation and failure process and the final shape of rock mass, which is mainly manifested as lap failure between joints. By comparing the 25 stress-strain curves obtained from the test, the stress-strain curves are classified into five types. With the increase of the normal stress, the composite shear type gradually transforms to the shear type, and the shear type gradually transforms to the yield type. The joint distribution pattern has a great influence on the shear strength and the maximum difference is 64 %.

### Key words:

jointed rock mass, joint distribution, shear test, mechanical behaviour, failure process

Prethodno priopćenje

**Xing-Chao Lin, Gui-Na Zhu, Xing-Song Sun**

## Mehaničko ponašanje stijenske mase pri ispitivanju smicanja simuliranih materijala

U ovom se radu proučava utjecaj raspodjele pukotina na karakteristike deformacije i čvrstoće stijenske mase kroz pokus izravnog smicanja pet tipičnih vrsta raspodjele simuliranih materijala koji uključuju dvije pukotine. Prostorni raspored pukotina određuje proces deformacije i loma te konačni oblik stijenske mase, koji se uglavnom očituje kao slom između pukotina. Usporedbom 25 naponsko-deformacijskih krivulja dobivenih ispitivanjem, one se razvrstavaju u pet tipova. S povećanjem normalnog naprežanja kompozitni posmični tip postupno prelazi u posmični tip, a posmični tip postupno prelazi u tip popuštanja. Raspored pukotina ima velik utjecaj na posmičnu čvrstoću i maksimalna razlika je 64 %.

### Ključne riječi:

razlomljena stijenska masa, raspodjela pukotina, pokus izravnog smicanja, mehaničko ponašanje, proces loma

### 1. Introduction

Rock masses are formed by long-term geological conformation movement and contain a large number of discontinuities, such as faults, joints, bedding plates, and fissures. These discontinuities intersect, developing a specific rock mass structure. This way, the failure mechanism of a rock mass and its engineering mechanical properties, such as strength and deformation, are determined by the complicated structure. A substantial number of engineering studies have verified that the deformation, failure, and instability of a rock mass are usually caused by the deformation, failure, propagation and even coalescence of joints inside the rock mass [1-4]. From this point of view, it is of great significance to study the influence of the distribution characteristics of joints on the mechanical properties of a jointed rock mass.

The physical model test of prefabricated joints is an effective means to study the influence of structural planes on the mechanical properties of jointed rock mass, mainly including uniaxial compression test, direct shear test, etc. There are many research results on the laboratory model test of prefabricated jointed rock mass in the former studies [5-25]. Due to the limitation of test conditions, whether it is uniaxial compression test or direct shear test, the jointed rock mass samples in the above-mentioned studies are mainly single group parallel joints or specific combinations, which prove difficult to truly reflect the real failure characteristics of complex jointed rock mass.

Wang et al. [7] obtained more than 100,000 measured data of structural planes during the construction of 35 hydropower projects. Based on these data, five typical structural plane distribution patterns (Fig. 1) were summarized through statistical analysis. Most structural plane distributions can be derived from these five distribution patterns, which can better reflect the structural characteristics of rock mass.

In this paper, by making a typical jointed rock mass modelling device, optimizing the test and testing system, and designing the overall test scheme, the direct shear test study was carried out on the above-mentioned five types of jointed rock mass with

typical joint distribution patterns and two joints. The process of deformation, expansion and failure of jointed rock mass under the condition of typical structural plane distribution patterns is analyzed. Additionally, the mechanism of different joint distribution patterns on the comprehensive shear strength is revealed.

### 2. Experimental methodology

#### 2.1. Sample preparation

The jointed rock samples were made from a mixture of plaster, water, cement and sand in certain proportions. Rocks with different strengths can be obtained by adjusting the material proportions in the mixture. Moreover, steel sheets and abrasive papers were buried in the pouring process to simulate the joints. The characteristics of different joints could be simulated by altering the thickness of the built-in fitting, processing modes and materials. The physical model construction process and control points are presented as follows:

- The mass proportion used in the test was sand: cement: water = 3: 2: 1.13. A small concrete mixer was used to mix the materials, as shown in Fig. 2.a.
- An iron sheet with a thickness of 0.7 mm was used as a joint forming tool, as shown in Fig. 2.b and 2.c. A comparison test was conducted to determine when the iron sheet could be pulled out easily without breaking the geometric morphology of the joint, and 8 hours after model pouring was found to be the best timing.
- The dimensions of the joint model were 300 × 300 × 150 mm (length × width × height). All samples must be produced simultaneously to maintain the conformity of the test materials. The sample moulds used in this study are shown in Fig. 2.d and 2.e.
- The moulds were removed 2 days after the sample pouring was completed and then the samples were cured for 21 days at room temperature before testing. The characteristic parameters of the rock mass and the joint were determined through direct shear tests and the results are listed in Table 1.

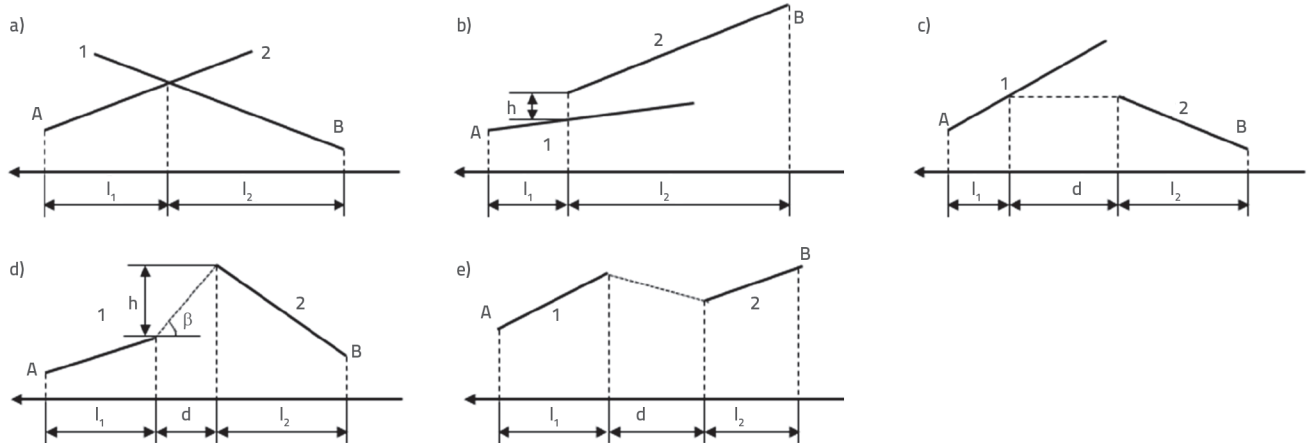


Figure 1. Five basic combination forms of joints and rock bridges [26]

Table 1. Physical and mechanical parameters of the rock mass and joint

Materials	Elastic modulus [GPa]	Poisson's ratio	Friction angle [°]	Cohesion c [MPa]	Density [kg/m <sup>3</sup> ]
Rock	3.5	0.16	39.8	2.71	2100
Joint	-	-	30.8	0.59	-

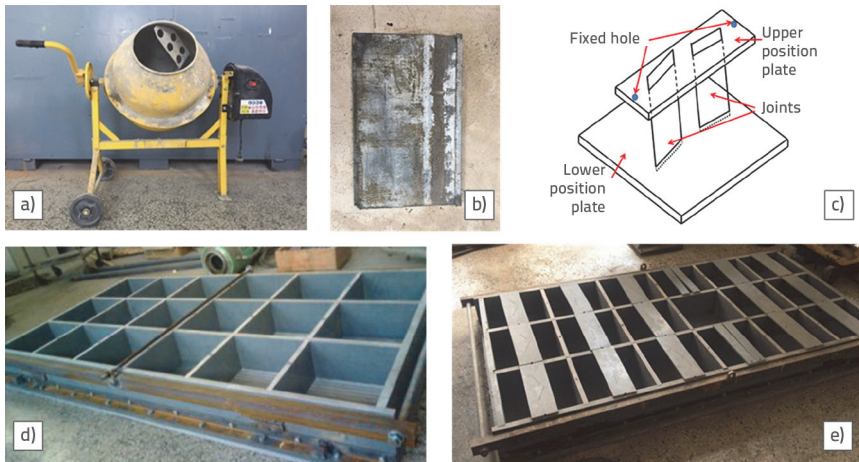


Figure 2. Sample preparation

2.2. Joint geometry design

In this paper, the jointed rock samples are designed in accordance with the distribution patterns proposed by Wang, X.G. et al. [26]. The specific geometric dimensions of the samples are shown in Fig. 3. In these figures, the starting and end points of joint

1 are B and C, respectively, whereas the starting and end points of joint 2 are D and E, respectively. The starting and end points of the shear test are A and F, respectively.

2.3. Testing procedure

An SAJM-2000 hydraulic servo rock universal testing machine is used as the test instrument (Fig. 4). After the sample is mounted on the shear framework, the shear framework is moved into the test machine host to realize simultaneous loading of the normal load and the shear load. The normal loading of the direct shear is controlled by force. A normal force of 5 kN is first loaded before the loading tests of corresponding loading levels. Note that the tangential loading is first controlled by the test force. A test force of 3 kN is preloaded and then converted into displacement control at a displacement rate of 0.5 mm/min. A camera fitted in the

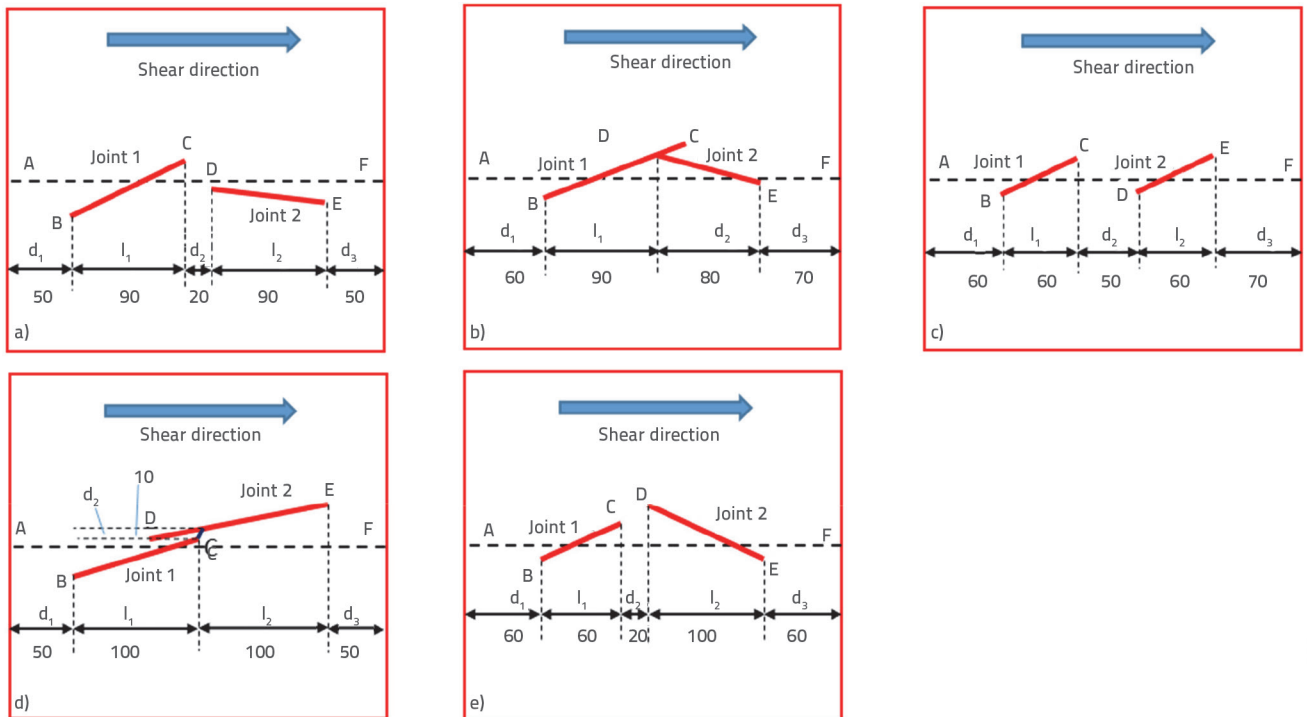


Figure 3. Physical dimensions of the samples (units [mm])

framework (Fig. 4) was used to record the sample failure process during testing. Additionally, a screen recording procedure was adopted to simultaneously record the failure process and the test stress-strain data. With this setup, the relevant characteristics of the test failure process and the mechanical characteristic curve can be observed repeatedly.

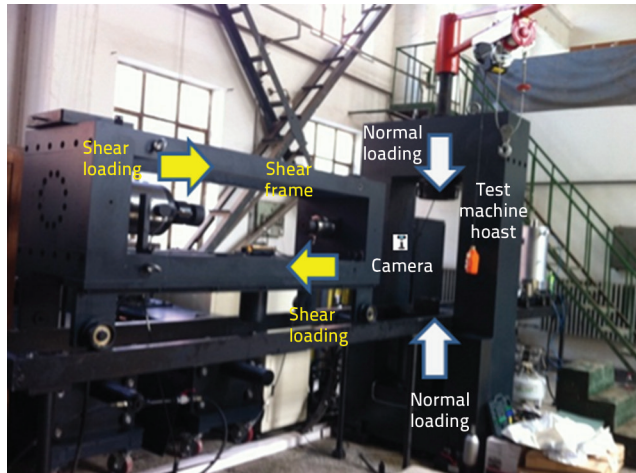


Figure 4. SAJM-2000 hydraulic servo rock universal test machine

Direct shear tests under different normal loads (0.5 MPa, 1.0 MPa, 1.5 MPa, 2.0 MPa, and 2.5 MPa) are carried out on the five types of rock mass models. A total of 25 direct shear tests are conducted on the rock mass models to study the evolution process and the strength characteristics of the jointed rock failure.

### 3. Results and analyses

#### 3.1. Stress-strain curves of rocks with various two-joint distributions under shear

The stress-strain curve of the samples can be obtained through a direct shear test. When the normal stress is 1.0 MPa, the stress-strain curves of various types of jointed rocks can be divided into the following stages (as shown in Fig. 5). The division and mechanical mechanism of these five stages are as follows:

1. Adjustment stage (oa). The shear load increases with increasing shear deformation, and the rate of change increases gradually. The mechanical mechanism of this stage is as follows: at the beginning of loading, there may be a small gap and angular deviation between the specimen and the shear frame. Under the action of shear loading, the specimen will produce elastic deformation and simultaneously produce compaction and adjustment deformation. When the shear load disappears, the elastic deformation will also disappear, but the compaction and adjustment deformation will remain; the specimen itself does not deform. The specimen is in the elastic stage. As shown in Fig. 5, the maximum distance below the line  $\overline{oc}$  is point a.

2. Linear elastic deformation stage (ab). The shear load increases with increasing shear deformation, and the rate of change remains constant. The mechanism of this stage is as follows: as the test continues, the shear stress increases with increasing displacement; when the shear load disappears, the deformation will also disappear. The specimen is in the elastic stage. The maximum distance above the line segment  $\overline{oc}$  is point b.
3. Invisible crack stage (bc). The shear load increases with increasing shear deformation, and the rate of change decreases gradually. The forming mechanism of this stage is as follows: when the shear load is close to the peak strength of the jointed rock mass, local plastic deformation may occur at the joint tip and the loading position. When the shear load disappears, this part of displacement cannot be completely recovered, and the local part of the specimen is in the plastic stage. The point corresponding to the maximum value of shear resistance is c.
4. Crack propagation (cd). With increasing shear displacement, the shear load gradually decreases from the peak strength to the residual strength, and the stress path is related to the failure rate of the jointed rock mass. When the shear load reaches the peak strength, the fracture of the jointed rock mass occurs and cracks gradually expand until the joint has broken through, and the shear strength of the jointed rock mass gradually decreases until reaching the residual strength. Due to the appearance of cracks, the specimen will deform along the shear direction. When the deformation rate is higher than the loading rate of the test instrument, the stress drop phenomenon will appear, as shown in Fig. 5.a, 5.c to 5.e. When the deformation rate is sufficiently high, the shear load may be less than the residual strength of the jointed rock mass and then gradually increase to the residual strength in the test, as shown in Fig. 5.e. Point d is determined according to the failure process of the sample.
5. Residual deformation stage (de). With increasing shear displacement, the shear load does not change. The mechanism of forming the mechanical characteristics of this stage is as follows: the jointed rock mass has been broken through, and its characteristics are similar to the shear test results of joints with large fluctuations.

Compared with the previous direct shear test results of rock mass and joint [27-30], due to the structural characteristics of jointed rock mass, the stress-strain curve shows various forms in the crack propagation stage. The response curves in the jointed rock failure propagation stage can be split into sliding type, yielding type, shearing type, fracturing type and shearing combination type.

- Sliding type: In the direct shear test of a smooth straight joint, there is no crack propagation (cd) in the stress-strain curve (Fig. 6.a);
- Yielding type: The stress-strain curve is smooth as a whole, without any obvious decline in the crack propagation (cd), and is the most common type (Fig. 6.b);

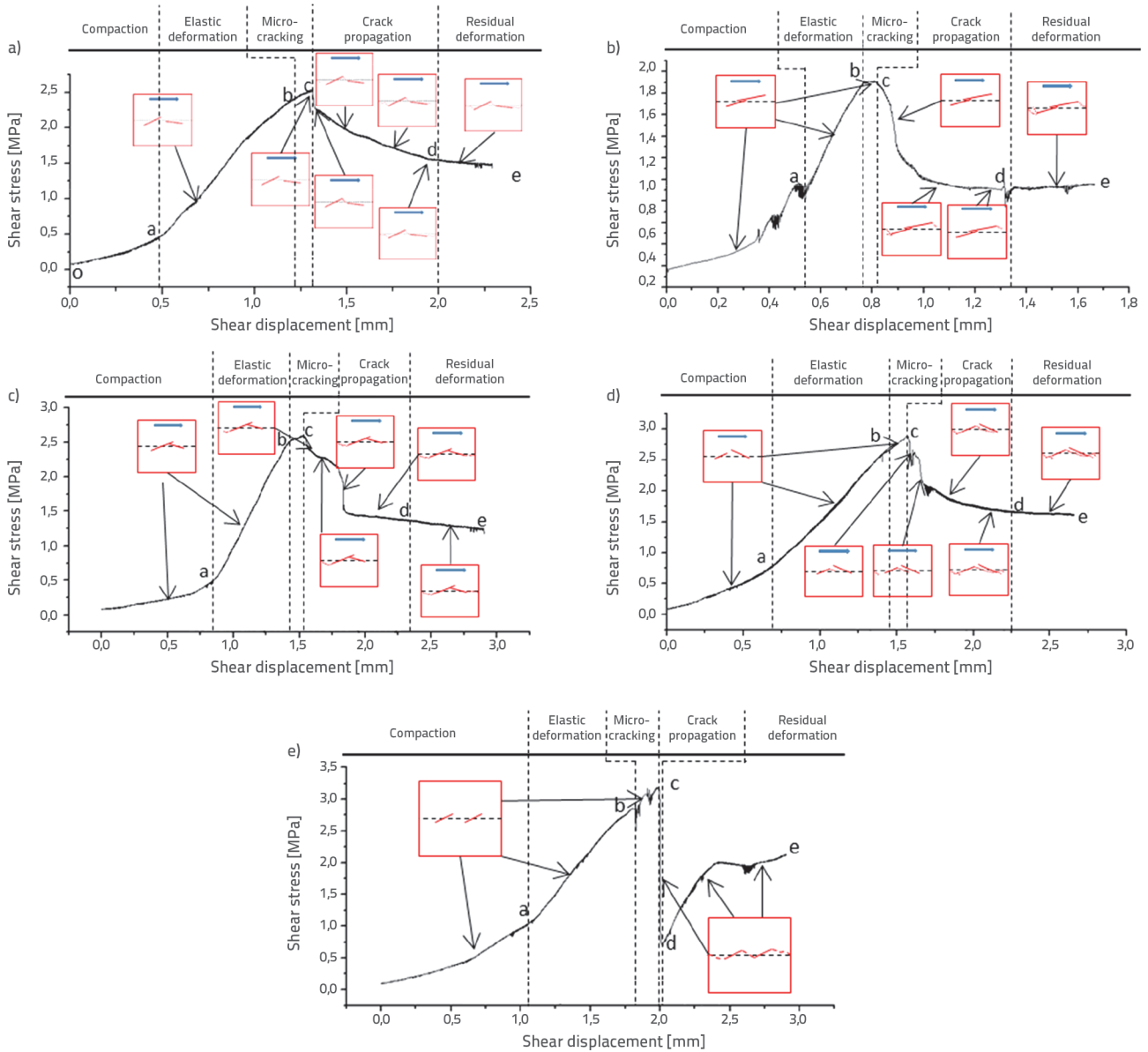


Figure 5. Failure processes of jointed rocks in typical distribution patterns

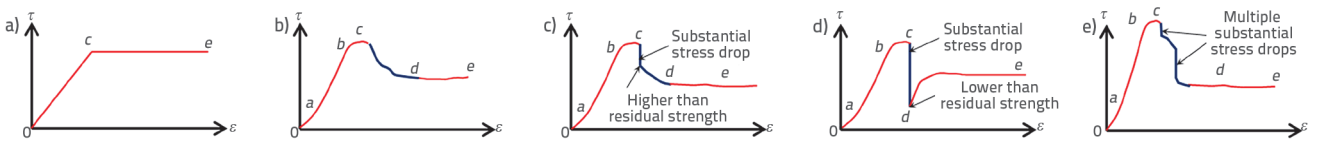
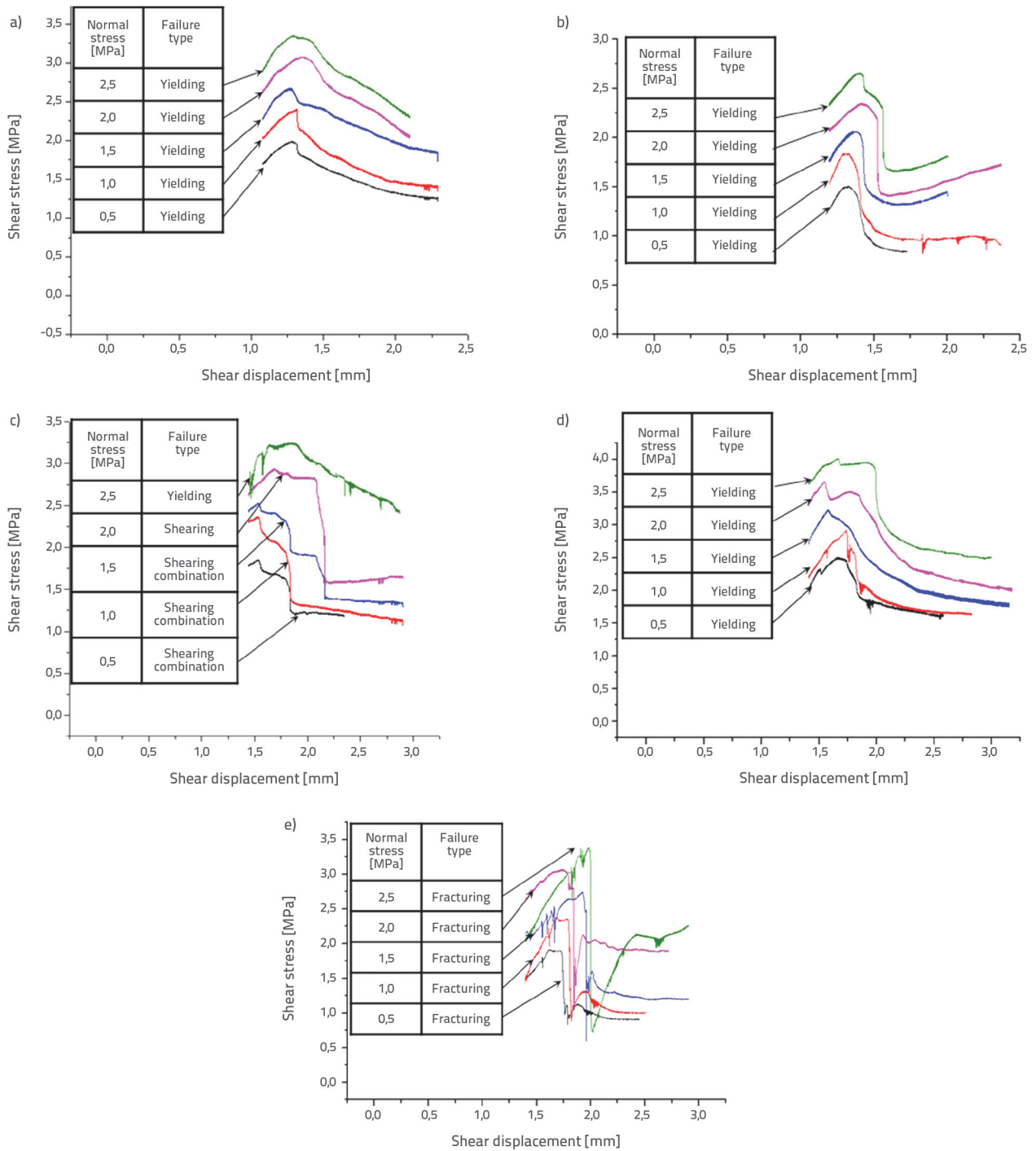


Figure 6. Division of stages in the stress-strain curves for various jointed rocks under a normal stress of 1.0 MPa

- Shearing type: The stress-strain curve is smooth as a whole in the early stage, has a substantial stress drop when reaching the peak strength, and reaches the residual strength when the stress becomes small after dropping. There is a stress drop over 5 % (Fig. 6.c);
- Fracturing type: The stress-strain curve is smooth as a whole in the early stage, has a substantial stress drop when reaching the peak strength, and reaches the residual strength along with increasing stress in the later stage. There is a stress drop of more than 20 % (Fig. 6.d);
- Shearing combination type: The stress-strain curve is smooth as a whole in the early stage, has multiple substantial stress drops after reaching the peak strength and reaches the residual strength along with decreasing stress in the later stage. There are several stress drops over 5 % (Fig. 6.e).



**Figure 7. Division of stages in the stress-strain curves for various jointed rocks under different normal stress conditions**

To understand the mechanical response characteristics of the jointed rock samples in the failure process, the stress-strain curves of the five typical joint distribution samples under different normal loading conditions are depicted together (after invisible crack stage), as shown in Fig. 7.

The data in the Fig. 7 clearly shows that the joints distribution in the rock mass plays a controlling effect in the specific types of jointed rocks. With increasing normal loading, the different types

jointed rock masses show the following different mechanical characteristics:

For type I, type II, type III and type IV, the larger the normal stress is, the combined shearing type will be transformed to the shearing type, whereas the shearing type will be transformed to the yielding type.

For type V, larger the normal stress is, the higher the shear strength of the jointed rock mass. The more obvious the stress

drop phenomenon that occurs when the failure occurs. The failure type remains a brittle fracture type.

The reason for the above phenomenon is that the failure process of type I, type II, type III and type IV is progressive failure, the larger the normal stress is, the more obvious the limiting effect of crack growth, the less likely it is to produce substantial stress drop; The failure process of type V is sudden failure, the greater the normal stress is, the greater the accumulated energy is, the greater the energy released during the failure is, and the more substantial the stress drop phenomenon is.

### 3.2. Failure process and modes

For the samples with identical joint distribution patterns, their failure processes are consistent under different normal stress conditions. The shear strength and the sketch of the failure process in the failure, propagation and connection processes of the joint samples under a normal stress of 1.0 MPa are provided due to space limitations, as shown in Table 2 to Table 6.

The type I jointed rock, as shown in Table 2, is mainly characterized by progressive lapping failure between the jointed rock bridges. The joint failure, propagation and connection process can be clearly observed through the video. As the shear

loading continues, a partially removed surface can be observed on the sample, indicating the generation of internal microcracks when the shear load approaches the ultimate shear strength of the jointed rock. Subsequently, the rock bridge "CD" between the joints "BC" and "DE" fails suddenly accompanied by a weak sound and a decrease in shear load when the shear load reaches the ultimate shear strength of the jointed rock. As the loading continues, the shear starting point A gradually propagates to the starting point B of the joint "BC". Moreover, the joint "DE" propagates to the shear end point F until they are connected.

The type II jointed rock, as shown in Table 3, is also characterized by progressive lapping failure between the jointed rock bridges. As the shear test continues, the rock behaves in the same way as the type I joint rock. A partially removed surface can be observed on the sample, which is accompanied by the formation of microcracks when the shear load approaches the ultimate shear strength of the jointed rock. The starting point C of the joint "BC" propagates to the joint "DE" when the shear load reaches the ultimate shear strength of the jointed rock. No significant stress decrease can be detected in the type II jointed rock because of the close distance between point C and joint "DE". As the loading continues, the shear starting point A gradually propagates to the starting point B of the joint "BC".

Table 2. Failure processes of jointed rocks in type I

Video	Shear strength	Sketch

Table 3. Failure processes of jointed rocks in type II

Video	Shear strength	Sketch

Moreover, the joint "DE" propagates to the shear end point F until they are connected.

The type III jointed rock, as shown in Table 4, is also characterized by progressive lapping failure between the jointed rock bridges. When the shear load reaches the ultimate shear strength of the jointed rock, as the joint "BC" intersects the joint "DE", the shear starting point A gradually propagates to the starting point B of the joint "BC". Then, as the loading continues, the joint "DE" propagates to the shear end point F until they are connected.

The type IV jointed rock, as shown in Table 5, is characterized by progressive lapping failure among the joint "BC", the shear starting point A and the end point F, and the crack propagated over the joint "DE". When the shear load reaches the ultimate shear strength of the jointed rock, the shear starting point A gradually propagates to the starting point B of the joint "BC", and the end point C of the joint "BC" propagates and ultimately connects to the shear end point F.

The type V jointed rock, as shown in Table 6, is characterized by sudden lapping failure between the jointed rock bridges. Unlike the jointed rocks in the other patterns, when the shear load reaches the ultimate shear strength of the jointed rock, the shear starting point A to the starting point of the joint "BC", the

ending point C of the joint "BC" to the starting point D of the joint "DE", and the end point E of the joint "DE" to the shear end point F fail simultaneously, causing obvious decreases in shear loading and emanating loud sounds.

Note: The sample images and loading curves in Table 2 on the left of the figures are screenshots from the video. The panorama of the sample can only be captured by a wide-angle camera due to the space limitations of the test machine. Because wide-angle shooting leads to distortion, a sketch of the image after eliminating this distortion effect is shown on the right of the figures.

Under different normal stress conditions (0.5 MPa, 1.0 MPa, 1.5 MPa, 2.0 MPa, and 2.5 MPa), the failure processes of the five types of jointed rocks are basically consistent. The failure and propagation processes of the joint rock are determined by the jointed distribution pattern. Type I, II, and III jointed rocks are mainly characterized by progressive lapping joint failure between the jointed rock bridges. Type IV is characterized by the progressive lapping failure among the joint "BC", the shear starting point A and the end point F. Type V jointed rock is characterized by sudden lapping failure between the jointed rock bridges.

Table 4. Failure processes of jointed rocks in type III

Video	Shear strength	Sketch
<p>B → A crack appear</p>		
<p>E → C crack appear</p> <p>E → F crack appear</p>		

Table 5. Failure processes of jointed rocks in type IV

Video	Shear strength	Sketch
<p>A → B crack appear</p>		
<p>A → B crack penetration</p> <p>E → F crack appear</p>		
<p>C → F crack penetration</p>		

Table 6. Failure processes of jointed rocks in type V

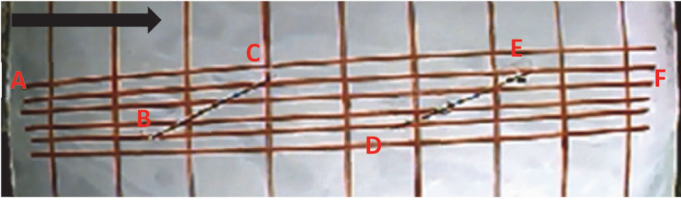
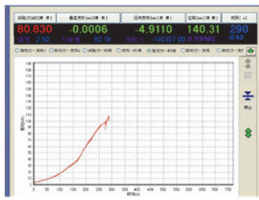
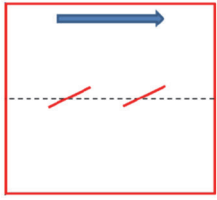
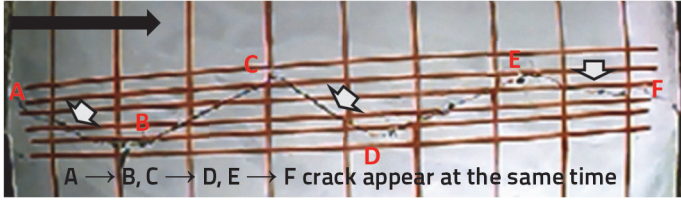
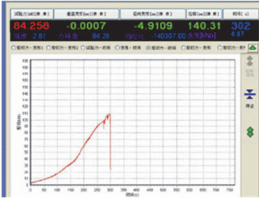
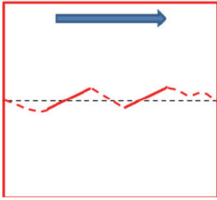
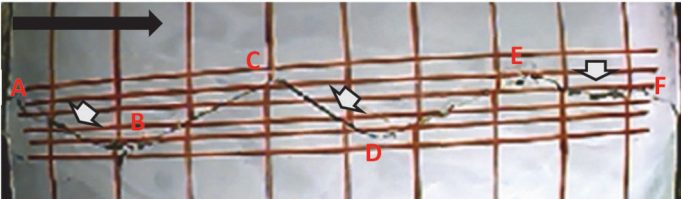
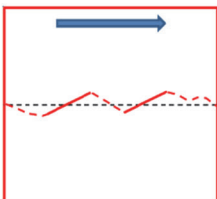
Video	Shear strength	Sketch
		
		
		

Table 7. Statistics of final failure modes of jointed rocks in typical distribution patterns

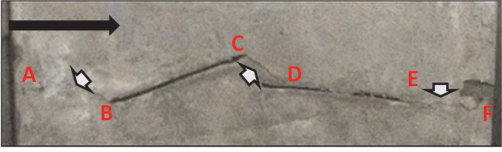
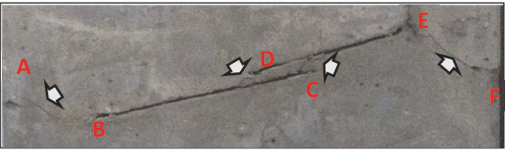
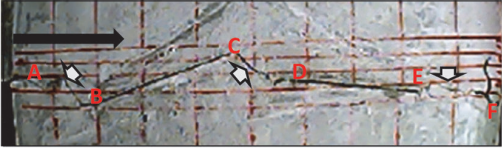
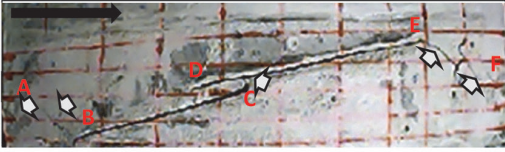
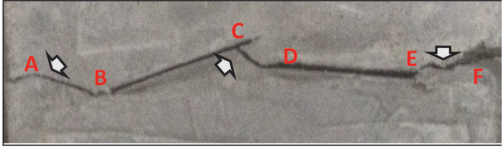
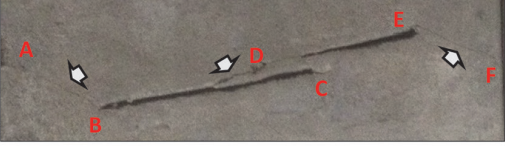
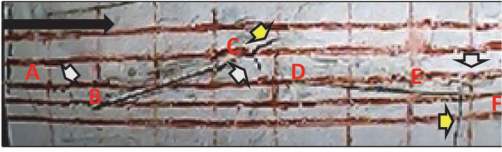
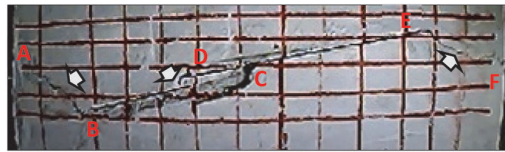
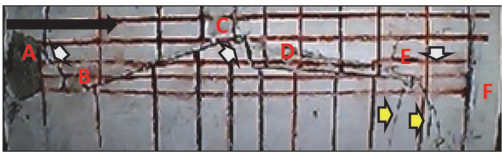
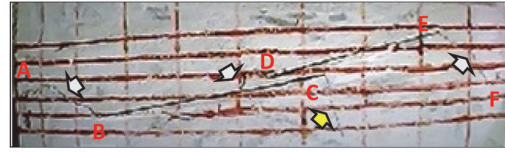
Normal stress [MPa]	Type I	Type II
0.5		
1.0		
1.5		
2.0		
2.5		

Table 7. Statistics of final failure modes of jointed rocks in typical distribution patterns - continuation

Normal stress [MPa]	Type III	Type IV
0.5		
1.0		
1.5		
2.0		
2.5		
Normal stress [MPa]	Type V	Note
0.5		<p data-bbox="905 1556 1201 1588">◻ Cracks in the main failure path</p> <p data-bbox="905 1608 1085 1640">◼ Secondary cracks</p>
1.0		
1.5		
2.0		
2.5		

When the normal stresses are 0.5 MPa, 1.0 MPa, 1.5 MPa, 2.0 MPa and 2.5 MPa, the ultimate failure modes of the five samples in the typical distribution patterns are summarized in Table 7. Based on Table 7, we can identify the following characteristics:

- The lapping joint failure between two joints is a major failure pattern in the direct shear test of jointed rocks in the typical distribution patterns.
- The type IV joint rock directly crosses the joint "DE" because the tensile failure strength between the end point C of the joint "BC" and the shear end point F is less than the combined shear strength of "C->D->E->F". Hence, the ultimate failure mode of the rock is determined by the distribution features of the joint.
- Under different normal stress conditions, when the failure modes of the jointed rocks are identical, slight differences might exist in the lapping positions between the two joints.
- Under high normal stress conditions, the wing cracks that in uniaxial compression tests might also occur at the joint tip, which exerts no influence on the primary failure path of the jointed rock.

### 4. Shear strength of rocks with various two-joint distributions

The shear strength index of a jointed rock, which is a significant basis for engineering design, is directly related to the economics and security of an engineering application; hence, this index has been frequently studied by scholars worldwide. Under different normal stresses, three failure modes, including tensile failure, shear failure and compression-shear failure, that might take place in a rock bridge have been proposed in accordance with experimental research and theoretical analysis. By summarizing

Lajtai's research achievements, [21-23]. Lajtai proposed that the failure type of a rock bridge should be determined according to the shear direction and the inclination of the rock bridge (Fig. 8); moreover, they derived the following calculation method for the shear strength:

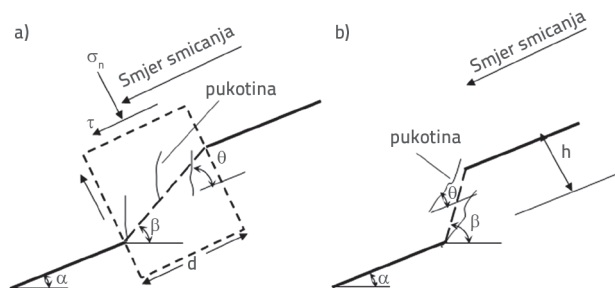


Figure 8. Relationship between the shearing direction and the inclined angle of the rock bridge

As shown in Fig. 8,  $\alpha$  is the angle of the joint,  $\beta$  is the angle of the connecting path between two joints, and  $\theta$  is the angle between the joint and the crack. When  $\beta < \alpha + \theta$ , shear and tensile failure will occur at the rock bridge, and the comprehensive shear strength  $R_r$  is calculated with Eq. (1).

$$R_r = \tau_r d = \sqrt{\sigma_t(\sigma_t + \sigma_n)} d \tag{1}$$

When  $\beta > \alpha + \theta$ , tensile failure will occur at the rock bridge, and the comprehensive shear strength  $R_r$  is calculated with Eq. (2).

$$R_r = \sigma_t d \tag{2}$$

Table 8. Comparison between theoretical and experimental results of shear strength of jointed rock masses

Results and errors	Normal stress [MPa]					Type
	0.5	1.0	1.5	2.0	2.5	
Test results [MPa]	1.99	2.41	2.67	3.07	3.35	I
By Equation (3) [MPa]	1.94	2.24	2.61	3.11	3.60	
Error [%]	-2.34	-6.95	-2.23	1.14	7.45	
Test results [MPa]	1.85	2.37	2.53	2.94	3.25	II
By Equation (3) [MPa]	1.88	2.18	2.52	3.00	3.49	
Error [%]	1.68	-8.10	-0.43	2.14	7.29	
Test results [MPa]	1.91	2.38	2.75	3.07	3.39	III
By Equation (3) [MPa]	1.96	2.20	2.62	3.15	3.65	
Error [%]	2.51	-7.56	-4.80	2.48	7.73	
Test results [MPa]	1.52	1.86	2.09	2.37	2.68	IV
By Equation (3) [MPa]	1.41	1.89	2.25	2.53	2.80	
Error [%]	-7.43	1.61	7.51	6.77	4.61	
Test results [MPa]	2.49	2.90	3.21	3.64	3.99	V
By Equation (3) [MPa]	2.35	2.70	3.12	3.73	4.32	
Error [%]	-5.66	-6.90	-2.85	2.36	8.27	

Based on Lajtai's strength theory and the research by [10, 26], presented five basic forms of jointed rock bridges (Fig. 1) with corresponding calculation equations. The comprehensive shear strength  $R_r$  is calculated with the following expression (3):

$$R_r = \sum \tau_{ji} l_i + \sum \tau_{ri} d_i \quad (3)$$

where  $\tau_{ji}$  and  $l_i$  are the shear strength of the  $i$ th joint and the projection of the joint on the horizontal plane, respectively, and  $\tau_{ri}$  and  $d_i$  are the shear strength (or tensile strength) and the projection length of the  $i$ th rock bridge, respectively. When  $\beta < \alpha + \theta$ ,  $\tau_{ri} = \sqrt{\sigma_i(\sigma_i + \sigma_n)}$  and  $d_i$  is the projection of the rock bridge on the horizontal plane, as shown in Fig. 8.a. When  $\beta > \alpha + \theta$ ,  $\tau_{ri} = \sigma_t$  and  $d_i$  is the projection along the vertical direction of the joint, as shown in Fig. 8.b.

The above two strength theories could be verified by the strength of jointed rock samples with typical joints. The strength parameters of the jointed rock mass are listed in Table 1. Parameters of the strength of the joint can be obtained through direct testing with cut-through joints (Table 1). Geometric characteristic parameters of the joints are presented in Fig. 3, and the verification results are summarized in Table 8.

According to the data in Table 8, the shear strength characteristics of the rock mass with two joints are as follows:

- Under low normal stress (0.5 MPa, 1.0 MPa), the shear strength calculated with Eq. (3) is slightly lower than the test results. Under high normal stress, the shear strength calculated with Eq. (3) is slightly higher than the test results. The maximum error between the calculation and the test results is small, so the formula method can be used to calculate the shear strength of the jointed rock mass.
- For the typical jointed rock mass and rock bridge overlapping failure type, the failure strength is determined by the shear rock bridge distance (type I, type II, type III, and type V). The shear strength of these sample types from greatest to least is type V > type I > type III > type III, and the same tip rock bridge length is 180 mm, 120 mm, 110 mm, and 100 mm, respectively. For the type IV jointed rock mass, the shear strength of the rock bridge is lower than that of the other types of jointed rock mass due to its tensile failure. The distribution of joints in the jointed rock mass controls the

shear strength of the rock mass.

## 5. Conclusion

Laboratory direct shear tests in combination with a developed typical jointed rock system modelling device, experimental test system optimization and an overall testing programme design were conducted to obtain a series of videos and test data. These results not only provided a foundation for studying the failure process, the failure mode and the mechanical response mechanism of the jointed rock but also offered a test basis for simulating the deformation, propagation and failure of the jointed rock. The following conclusions can be drawn according to the 25 direct shear tests with the 5 typical jointed rocks.

The deformation, failure, and evolution of rock masses with typical joint distribution patterns were characterized by lapping failures between joints and rock bridges. Under different normal stress conditions, the spatial distribution pattern of the joints controlled the failure mode and process for the same types of jointed rocks. The stress-strain curves of the samples with typical joint distributions obtained through direct shear tests can be divided into adjustment compaction, linear elastic deformation, invisible cracking, microcracking, crack propagation, and residual deformation stages.

After comparing the 25 stress-strain full-process curves obtained from the tests, the stress-strain curves can be reduced to sliding, yielding, shearing, fracturing, and shearing combination types in accordance with the distribution characteristics of various types of stress-strain curves. The type of curve was determined by the joint distribution pattern and the normal stress conditions. As the normal stress increased, the shearing combination type transformed to the shearing type, and the shearing type transformed to the yielding type.

The joint distribution pattern has a great influence on the shear strength, and the maximum difference is 64 %. The distribution of joints in the jointed rock mass controlled the shear strength of the rock mass.

## Acknowledgements

This research was supported by the National Key R&D Program of China (No. 2018YFC0407000), the National Natural Science Foundation of China (No. 51809289) and the IWHR Research & Development Support Program (Nos. GE0145B462017 and GE0145B692017). Research Project of China Three Gorges Corporation (Contract No. JG/19055).

## REFERENCES

- [1] Hoek, E., Bray, J.D.: Rock slope engineering, The Institution of Mining and Metallurgy, London, 1977.
- [2] Hoek, E., Diederichs, M.S.: Empirical estimation of rock mass modulus, *Int. J. Rock. Mech. Min. Sci.*, 43 (2006) 2, pp. 203–215
- [3] Tang, C.A., et al.: Analysis of crack coalescence in rock-like materials containing three flaws-Part II: numerical approach, *Int. J. Rock. Mech. Min. Sci.*, 38 (2001) 7, pp. 925–939
- [4] Henshell, R.D., Shaw, K.G.: Crack tip finite elements are unnecessary, *Int. J. Numer. Methods. Eng.*, 9 (2010) 3, pp. 495–507
- [5] Zhang, B., et al.: Uniaxial compression mechanical property test, fracture and damage analysis of similar material of jointed rock mass with filled cracks, *Rock Soil. Mech.*, 33 (2012) 6, pp. 1647–1652

- [6] Bahaaddini, M., et al.: Scale effect on the shear behaviour of rock joints based on a numerical study, *Eng. Geol.*, 181 (2014), pp. 212-223
- [7] Wang, L.H., et al.: Study of non-consecutive jointed rock mass under uniaxial compression, *J. Hydraul. Eng.*, 45 (2014) 12, pp. 1410-1418
- [8] Huang, C., et al.: Analysis of indoor uniaxial compression test on layered anisotropic rock masses, *J Yangtze River Sci. Res. Inst.*, (2016) 5, pp. 14
- [9] Ma, G.W., et al.: Modelling complex crack problems using the numerical manifold method, *Int. J. Fract.*, 156 (2009) 1, pp. 21-35
- [10] Einstein, H.H., Baecher, G.B.: Probabilistic and statistical methods in engineering geology, *Rock Mech. Rock. Eng.*, 16 (1983) 1, pp. 39-72
- [11] Einstein, H.H., Dershowitz, W.S.: Tensile and shear fracturing in predominantly compressive stress fields - A Review, *Eng. Geol.*, 29 (1990) 2, pp. 149-172
- [12] Shen, B., Stephansson, O.: Numerical analysis of mixed mode I and mode II fracture propagation, *Int. J. Rock. Mech. Min. Sci. Geomech. Abstr.*, 30 (1993) 7, pp. 861-867
- [13] Shen, B., Stephansson, O.: Modification of the G -criterion for crack propagation subjected to compression, *Eng. Fract. Mech.*, 47 (1994) 2, pp. 177-189
- [14] Shen, B.: The mechanism of fracture coalescence in compression: Experimental study and numerical simulation, *Eng. Fract. Mech.*, 51 (1995) 1, pp. 73-85
- [15] Chau, K.T. Wong, R.H.C.: Uniaxial compressive strength and point load strength of rocks, *Int. J. Rock. Mech. Min. Sci. Geomech. Abstr.*, 33 (1996) 2, pp. 183-188
- [16] Wong, R.H.C., Chau, K.T.: Crack coalescence in a rock-like material containing two cracks, *Int. J. Rock. Mech. Min. Sci.*, 35 (1998) 2, pp. 147-164
- [17] Chau, K.T., et al.: Fragmentation of brittle spheres under static and dynamic compressions: Experiments and analyses, *Mech. Mater.*, 32 (2000) 9, pp. 543-554
- [18] Wong, R.H.C., et al.: The mechanisms of crack propagation from surface 3-D fracture under uniaxial compression, *Key. Eng. Mater.*, 261-263 (2004) 1, pp. 219-224
- [19] Wong, R.H.C., Lin, P., Tang, C.A.: Experimental and numerical study on splitting failure of brittle solids containing single pore under uniaxial compression, *Mech. Mater.*, 38 (2006) 1, pp. 142-159
- [20] Chen, X.R., Liao, Z., Peng, X.: Deformability characteristics of jointed rock masses under uniaxial compression, *Int. J. Min. Sci. Technol.*, 22 (2012) 2, pp. 213-221
- [21] Lajtai, E.Z.: Shear strength of weakness planes in rock, *Int. J. Rock. Mech. Min. Sci. Geomech. Abstr.*, 6 (1969) 5, pp. 499-508, IN7-IN8, 509-515.
- [22] Lajtai, E.Z.: A theoretical and experimental evaluation of the Griffith theory of brittle fracture, *Tectonophysics*, 11 (1971) 2, pp. 129-156
- [23] Lajtai, E.Z.: Effect of tensile stress gradient on brittle fracture initiation, *Int. J. Rock. Mech. Min. Sci. Geomech. Abstr.*, 9 (1972) 5, pp. 569-578
- [24] Kulatilake, P.H.S.W., et al.: Analysis of structural homogeneity of rock masses, *Eng. Geol.*, 29 (1990) 3, pp. 195-211
- [25] Kulatilake, P.H.S.W., Fiedler, R., Panda, B.B.: Box fractal dimension as a measure of statistical homogeneity of jointed rock masses, *Eng. Geol.*, 48 (1997) 3-4, pp. 217-229
- [26] Wang, X.G., et al.: Determination of discontinuity persistent ratio by Monte-Carlo simulation and dynamic programming, *Eng. Geol.*, (2016) 203, pp. 83-98
- [27] Huang, T.H., Chang, C.S., Chao, C.Y.: Experimental and mathematical modeling for fracture of rock joint with regular asperities, *Engineering Fracture Mechanics*, 69 (2002) 17, pp. 1977-1996
- [28] Saiang, D., Malmgren, L., Nordlund, E.: Laboratory tests on shotcrete- Rock joints in direct shear, tension and compression, *Rock Mechanics & Rock Engineering*, 38 (2005) 4, pp. 275-297
- [29] Bahaaddini, M., et al.: Experimental and numerical study of asperity degradation in the direct shear test, *Engineering Geology*, 204 (2016), pp. 41-52
- [30] Zhu, J.B., Li, H., Deng, J.H.: A one-dimensional elastoplastic model for capturing the nonlinear shear behaviour of joints with triangular asperities based on direct shear tests, *Rock Mechanics and Rock Engineering*, 52 (2018), pp. 1671-1687